Long-Lived Charge Extraction in CsMAFA-Based Perovskites in n-i-p and p-i-n Structures

Zhao, Jiashang; van der Poll, Lara M.; Looman, Sander L.; Yan, Jin; Thieme, Jos; Ibrahim, Bahiya; Savenije, Tom J.

DOI
10.1021/acsenergylett.4c00250

Publication date
2024

Document Version
Final published version

Published in
ACS Energy Letters

ACS Energy LETTERS

http://pubs.acs.org/journal/aelccp

LETTER

Long-Lived Charge Extraction in CsMAFA-Based Perovskites in n-i-p and p-i-n Structures

Jiashang Zhao, Lara M. van der Poll, Sander L. Looman, Jin Yan, Jos Thieme, Bahiya Ibrahim, and Tom J. Savenije*

Cite This: *ACS Energy Lett.* 2024, 9, 2456−2463

Read Online

ACCESS | Metrics & More | Article Recommendations | Supporting Information

ABSTRACT: To increase the open-circuit voltage in solar cells based on triple cation, mixed halide perovskites, reducing recombination processes at the interfaces with transport layers (TLs) is key. Here, we investigated the charge carrier dynamics in bilayers and trilayers of $Cs_{0.05}MA_{0.10}FA_{0.85}Pb(I_{0.97}Br_{0.03})_3$ (CsMAFA) combined with TLs using time-resolved microwave conductance (TRMC) measurements without and with bias illumination (BI). In the bilayers, we find balanced mobilities for electrons and holes in CsMAFA and nearly quantitative carrier extraction. The small, rapidly decaying TRMC signals for n-i-p- and p-i-n triple layers indicate both carriers are extracted. Applying BI leads to the charging of the TLs and the corresponding electric field prevents additional charge extraction, which demonstrates long-lived charge separation over the CsMAFA/TLs. Most importantly, for all bilayer combinations showing long-lived charge separation, an increase of the quasi-Fermi level splitting with respect to that of the CsMAFA layer is found.

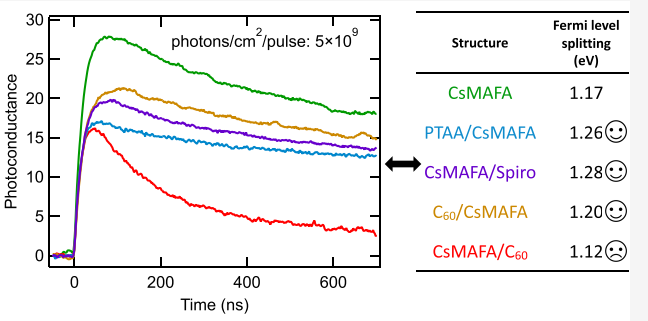

Structure	Fermi level splitting (eV)
CsMAFA	1.17
PTAA/CsMAFA	1.26 ☺
CsMAFA/Spiro	1.28 ☺
C_{60}/CsMAFA	1.20 ☺
CsMAFA/C_{60}	1.12 ☹

Metal halide perovskites (MHPs) have attracted worldwide attention in the past decade due to their excellent optoelectronic properties and to the rapidly increasing performance of MHP-based solar cells,[1−13] with recorded power conversion efficiencies of 26.1% in conventional n-i-p structures[14] and 24.6% in inverted p-i-n configurations.[15] Yet, despite this impressive progress in performance, to further reduce deficits between the obtained and maximum theoretical open-circuit voltage (V_{OC}),[16−18] it is crucial to understand the carrier dynamics including charge transport, extraction, and recombination at the interfaces. Photoluminescence quantum yield (PLQY) measurements revealing the quasi-Fermi level splitting (QFLS) in various MHP absorbers with hole or/and electron transport layers (TLs) show that nonradiative charge carrier recombination still occurs at most interfaces.[17,19,20] For this reason, an in-depth understanding of the carrier dynamics at the interfaces is of vital importance for further optimization.

Characterization of charge carrier dynamics at the interfaces has been investigated by employing various techniques ranging from laser spectroscopy to electrical measurements.[21−25] However, transient absorption or optically pump terahertz probe measurements are typically limited by the high excitation intensities required, leading to higher-order recombination processes and thus disguising the charge extraction.[26] Transient electrical measurements, such as transient photovoltage decay or intensity-modulated photocurrent/photovoltage spectroscopy on complete perovskite solar cells (PSCs) can elucidate carrier recombination mechanisms under operating conditions.[10,27] Nevertheless, the complexity of multiple interfaces at which various photophysical processes on different time scales occur in combination with undesired ion diffusion affecting the internal electric field makes the interpretation of such measurements very challenging.[28,29]

In this Letter, the contactless time-resolved microwave conductance (TRMC) technique was used to investigate carrier extraction and recombination at different interfaces in n-i-p and p-i-n stacks, by directly comparing the carrier dynamics in the perovskite absorber layer to those obtained in bilayer and trilayer systems. The structural, optical, and optoelectronic properties of CsMAFA are shown in Figure S1 and Note S1 in the Supporting Information for detailed discussion. In the first part of this Letter, by analyzing the TRMC traces recorded with various incident light intensities,

Received: January 24, 2024
Revised: March 27, 2024
Accepted: April 26, 2024
Published: May 1, 2024

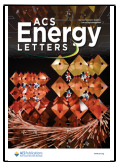

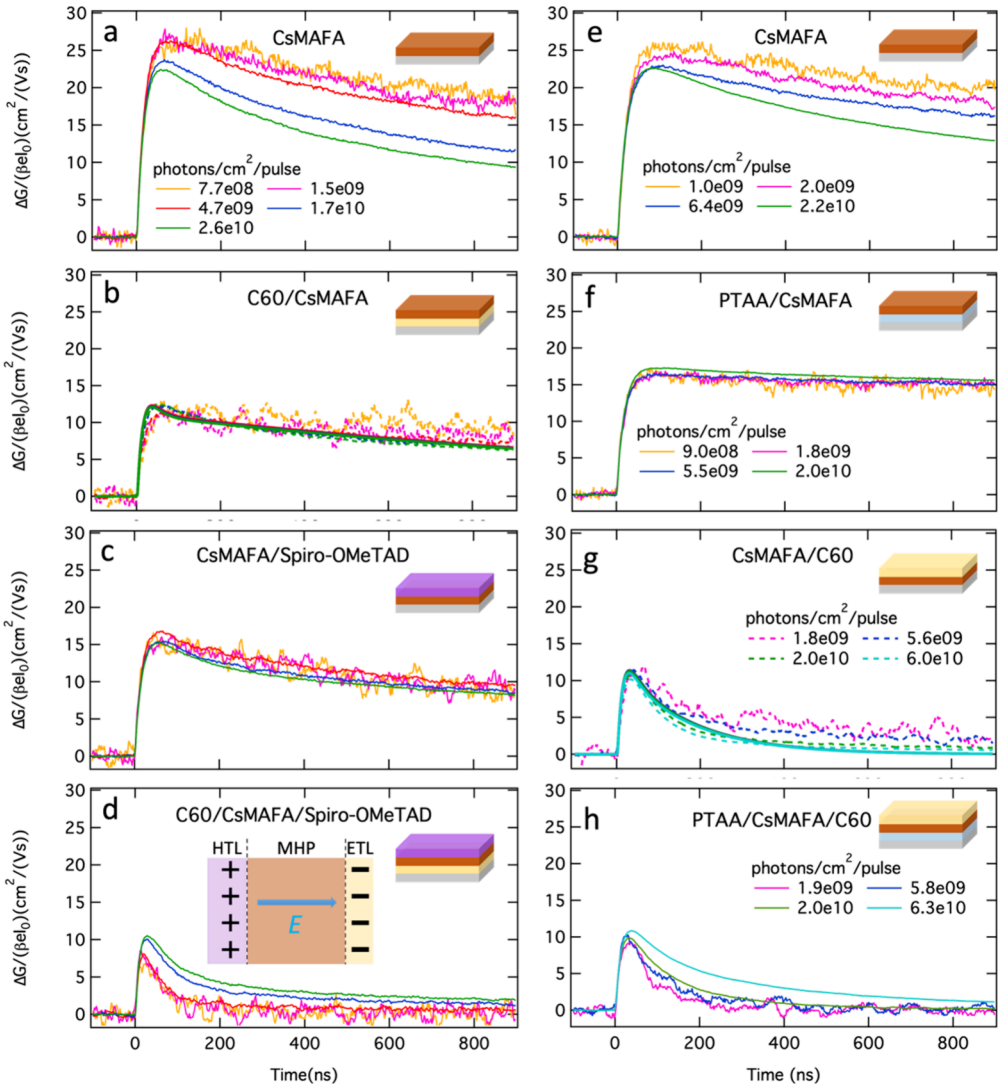

Figure 1. TRMC traces for CsMAFA (a), C60/CsMAFA (b), CsMAFA/Spiro-OMeTAD (c), C60/CsMAFA/Spiro-OMeTAD forming the n-i-p stack (d) and CsMAFA (e), PTAA/CsMAFA (f), CsMAFA/C60 (g), PTAA/CsMAFA/C60 forming the p-i-n stack (h) deposited on quartz (light gray). Traces are recorded on excitation at 650 nm with incident light intensities ranging from 10^9−10^{10} photons/cm^2/pulse. The fits for C60/CsMAFA and CsMAFA/C60 bilayers are indicated by the solid lines. A simplified parallel-plate capacitor illustrates the trilayer system after charge extraction in the inset. Note that the response time of the experiment is 18 ns, which will limit the rise of the TRMC traces (see Note S1 of the Supporting Information for more information).

we demonstrate that carrier extraction occurs in all bilayers and trilayers by the reduction of the TRMC signal height and the change in the decay kinetics. Furthermore, pulsed excitation in combination with bias illumination (BI) demonstrates long-lived carrier extraction over the CsMAFA/TL interfaces, as reflected by the almost comparable TRMC signals in bare CsMAFA and TL/CsMAFA/TL trilayers. Finally, we examine how charge collection and recombination at the interface affect the quasi-Fermi level splitting, which is derived from steady-state microwave conductivity (SSMC) measurements.

To investigate the charge collection from CsMAFA into the TLs, the charge carrier dynamics in neat CsMAFA were directly compared with those of the bilayers (TL/MHP or MHP/TL) and sandwich-like trilayers (TL/MHP/TL). Hence, two different types of stacks, i.e., n-i-p and p-i-n, were studied. First, we focused on the n-i-p architecture, where C60 was used as the electron TL (ETL) and Spiro-OMeTAD as the hole TL (HTL) (see Scheme S1 for energy band diagrams). For all systems, we excited samples using an excitation of 650 nm to ensure a homogeneous generation profile in CsMAFA (see Figure S2). More importantly, the absorption of TLs at 650 nm is negligible (see Figure S3), which means that the TRMC signal only originates from carriers initially generated in CsMAFA and is not affected by the parasitic absorption by the TLs.

First of all, on comparing the neat CsMAFA layer (Figure 1a) and bilayers (Figures 1b, c) in the n-i-p configuration, a substantial reduction in TRMC signal is observed in both bilayers, in agreement with our previous reports in $MAPbI_3$.[30,31] Since the mobility in TLs is at least 1 order of magnitude lower than in CsMAFA,[24] the reduced signal height implies that electrons and holes are injected into their respective layers while the remaining TRMC signal originates from carriers remaining in the perovskite (holes or electrons). Furthermore, we noticed that the sum of TRMC signals in bilayers (Figures 1b, c) is very similar to that in CsMAFA, suggesting that carriers were nearly completely transferred to their corresponding TLs. Moreover, it also demonstrates that

https://doi.org/10.1021/acsenergylett.4c00250
ACS Energy Lett. 2024, 9, 2456−2463

Scheme 1. (a) Kinetic Model of Charge Carrier Processes Initiated by Optical Excitation of CsMAFA[a] and (b) Illustration of Photo-Generated Carriers in CsMAFA under Pulsed Laser Combined with Bias Illumination[b]

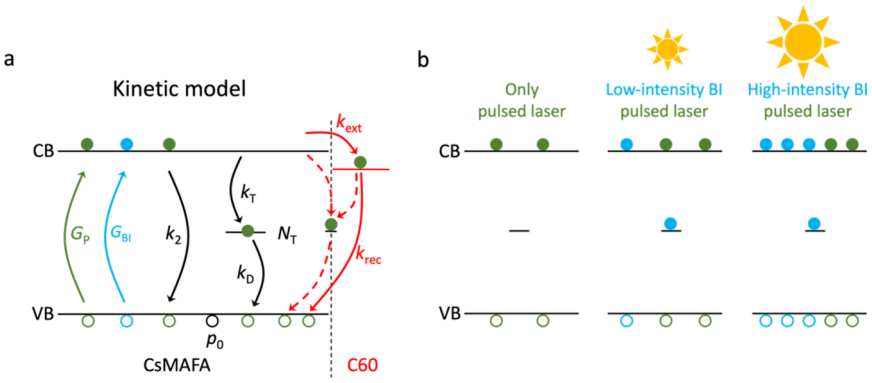

[a] G_P and G_{BI} represent the photo generation of charge carriers by pulsed laser alone or in combination with bias illumination (BI); k_2 depicts the second-order recombination rate. Electron trap-mediated recombination is described by trapping rate, k_T, and depopulation rate, k_D. Electrons are collected by C60 and consecutively recombined with holes in CsMAFA, represented by extraction rate k_{ext} and recombination rate k_{rec}, respectively (red arrows). [b] A BI arrives on the sample prior to the pulsed laser. Carriers generated by pulsed laser and BI are represented by green and light blue circles, respectively.

the electric field due to charge accumulation at the CsMAFA/TL interface does not yet hamper the charge collection. Additionally, the reduction in TRMC signal in both bilayers is comparable, indicating that their individual mobilities are similar, which means the difference is within 25%, consistent with what we previously reported.[32] Apart from the change in signal size, two additional observations can be noticed. First, for both bilayers, the lifetimes of the charge carriers are elongated in comparison to neat CsMAFA, which can be explained by the slow recombination of electrons and holes occurring over the interface since they are physically separated. Second, unlike in CsMAFA, all TRMC traces overlap at different intensities and have no second-order recombination features, meaning that in bilayers the carrier decay is dominated by first-order recombination via the interface. To address the reproducibility of our samples, TRMC traces of all single, bi- and trilayers from another batch are shown in Figure S4. On comparing those to Figure 1, the reduction in signal size in bilayers and trilayers is very similar, although some variation in the TRMC signal height of the bare perovskite layer is visible. Most importantly, the carrier decay dynamics are nearly identical for identical systems. Therefore, we believe this difference in signal height does not affect our conclusions that electrons and holes are efficiently injected into their respective layers and that the mobility of electrons and holes is similar.

Knowing that all these bilayers can efficiently extract carriers, it is of interest to examine how charge carriers in trilayer systems behave. As shown in Figure 1d, the TRMC traces recorded in the trilayer show a significant reduction in signal height, and the lifetimes of carriers are considerably shortened compared to both those of the single and bilayers. If complete extraction of carriers from CsMAFA to their respective TL happens rapidly in the trilayer, a very small, negligible TRMC signal should be expected due to the limited carrier mobility in the TLs. In reality, a small TRMC signal still remains. To examine whether the charge carrier diffusion time (τ) in CsMAFA is responsible for the remaining TRMC signal, we calculated τ across the CsMAFA film using the following equation:

$$L_D = \sqrt{\frac{k_B T}{e}\mu\tau} \quad (1)$$

where k_B is Boltzmann's constant, T is the absolute temperature, and e is the elementary charge. μ is the carrier mobility, here taken as 15 $cm^2/(Vs)$ in CsMAFA, and L_D is the diffusion length. Hence, assuming that L_D is equal to the thickness of the CsMAFA film of 500 nm, τ amounts to 6 ns. Although charge collection between CsMAFA and TLs is expected to be between picosecond and subnanosecond time scales, the actual extraction time of carriers is limited by carrier diffusion in CsMAFA. Since the response time of the microwave cavity used in this work is 18 ns, the effect of the instrumental response function (IRF) on the measured traces for a ΔG of 6 ns is shown in Figure S5, indicating that a small TRMC signal might still be retained. Most importantly, the short TRMC signal implies that almost complete carrier extraction occurs $I_0 < 5 \times 10^9$ photons/cm^2/pulse.

Furthermore, contrary to what we usually observe in single perovskite layers,[33,34] the intensity dependence in the trilayer exhibits longer charge carrier lifetimes and higher TRMC signals with increasing incident light intensities. One possible explanation for this increased signal is that the extracted charge carriers in their respective TLs give rise to an internal electric field in the trilayer system, as depicted in the inset of Figure 1d. The direction of this E-field is from the HTL toward the ETL, which is opposite to the carrier extraction, hindering further collection of carriers. It is worth noting that when $I_0 > 5 \times 10^9$ photons/cm^2/pulse, corresponding to a carrier density of 1×10^{13} cm^{-3}, this resulting electric field is sufficiently large to reduce further charge extraction.

Besides PSCs in conventional n-i-p architectures, inverted p-i-n PSCs have attracted more attention owing to their long operational stability derived from nondoped HTLs[15] and their successful integration with silicon solar cells into multijunction tandem solar cells.[35] Hence, also bilayers and trilayers with a p-i-n configuration were studied. Herein, we used PTAA as the HTL and C60 as the ETL. On comparing Figure 1e with 1f, corresponding to neat CsMAFA and PTAA/CsMAFA bilayer, a similar carrier decay behavior to that observed in the n-i-p structure is found upon introduction of the HTL, i.e. a

https://doi.org/10.1021/acsenergylett.4c00250
ACS Energy Lett. 2024, 9, 2456−2463

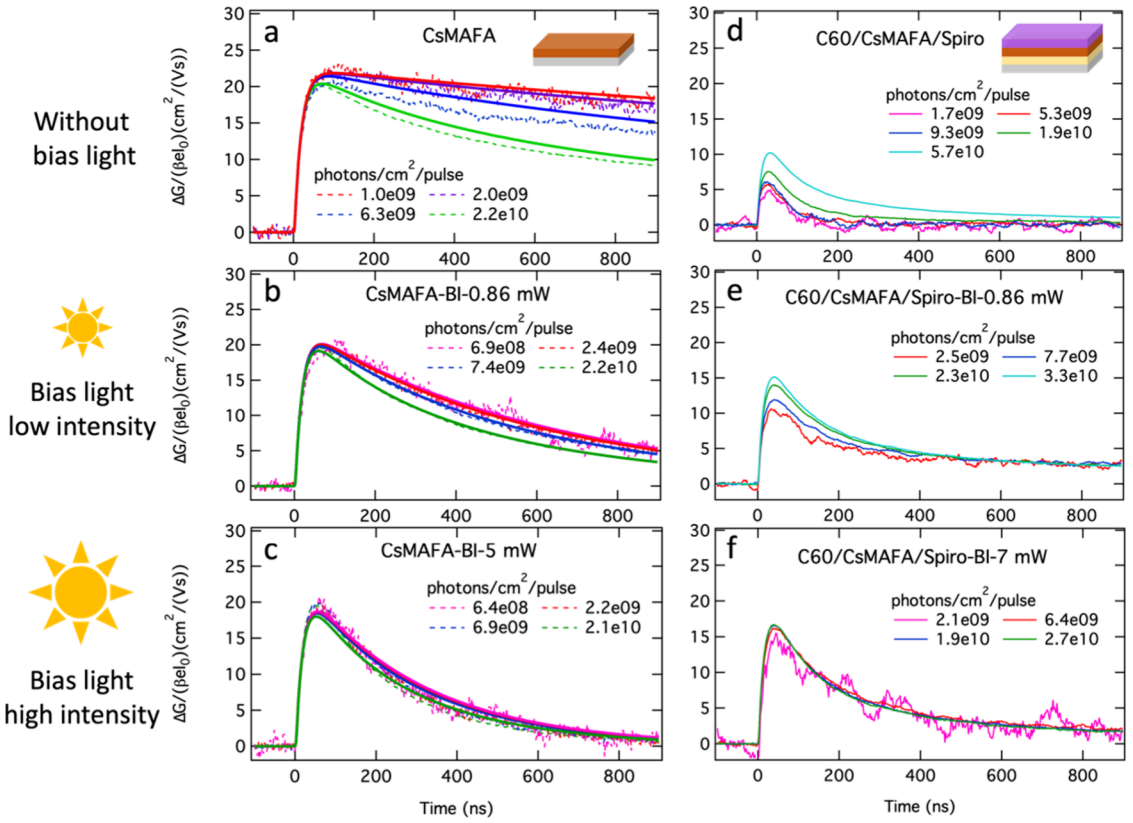

Figure 2. TRMC traces recorded in bare CsMAFA (left panels) and C60/CsMAFA/Spiro trilayer (right panels) deposited on quartz (light gray) without BI (a, d), with low-intensity BI (b, e) and high-intensity BI (c, f). For bare CsMAFA, the fits are added to the dashed experimental traces.

reduction in TRMC signal and an elongation of the lifetime of charge carriers. For the CsMAFA/C60 bilayer (Figure 1g), it is evident that charge extraction to C60 occurs, as shown by the drop in the maximum signal. However, only short-lived TRMC traces could be measured, possibly because C60 is not compatible with the CsMAFA top surface, leading to rapid interfacial recombination via a trap-assisted process (see Scheme 1a).[20] Nevertheless, in the PTAA/CsMAFA/C60 trilayer system (Figure 1h), the same features as in C60/CsMAFA/Spiro are observed.

To further verify the occurrence of long-lived charge extraction from CsMAFA to their respective TLs in the trilayers, we compared TRMC measurements of a bare CsMAFA layer with a C60/CsMAFA/Spiro trilayer under various bias illuminations (BI) using a white LED, as illustrated in Scheme 1b. A schematic representation of the TRMC setup and the protocol for conducting TRMC measurements with bias illumination are provided in Figure S6 and Figure S7 in the Supporting Information, respectively. The measured TRMC traces are shown in Figure 2. First, for the bare CsMAFA layer under 0.86 mW BI (corresponding to 0.04 sun) (Figure 2b), charge carrier decays become slightly faster and display less dominant second-order recombination. This can be attributed to the higher excess carrier concentration under BI. However, the concentration of excess carriers generated by the BI is still comparable to that generated by the pulsed illumination. When BI is increased to 5 mW (~ 0.3 sun), the decay is much faster and exhibits a pseudo-first-order recombination behavior, which indicates that carrier recombination is mainly governed by the charge carriers generated by the BI.

In contrast to neat CsMAFA, the trilayer system exhibits higher TRMC signals and longer carrier lifetimes with BI (Figures 2**d**, 2**e**, 2**f**). Using low-intensity BI (0.86 mW) the TRMC signals are increased by approximately 50% in comparison to that without BI. On further increasing the BI, the TRMC signal height is even higher and almost comparable to that in neat CsMAFA (compare Figures 2**c**, 2**f**). These observations can only be explained by the fact that under BI, charge extraction to the TLs occurs leading to a charge carrier equilibrium between CsMAFA and the TLs long before pulsed excitation. At low BI, the carriers in TLs are not saturated, and further charge extraction of carriers induced by the laser pulse can still take place to a certain degree. At high BI, the TLs appear to be almost saturated and no further charge extraction is feasible. Therefore, similar TRMC signals are observed in the single and triple layers under high BI. Then, the same TRMC measurements with BI were carried out on neat CsMAFA and PTAA/CsMAFA/C60 trilayer (p-i-n configuration, see Figure S8). For the CsMAFA single layer and trilayer, almost identical features are noticed as described above. It is worth mentioning that the charge carrier dynamics after removing the BI are very similar to the initial TRMC traces recorded with only the pulsed laser (see Figure S9). Hence these BI-induced changes are fully reversible and all perovskites and TLs are stable during BI.

To validate the above interpretation, we first modeled TRMC traces in bare CsMAFA without BI using the kinetic model (see Note S2 for the used set of differential equations

https://doi.org/10.1021/acsenergylett.4c00250
ACS Energy Lett. 2024, 9, 2456−2463

S5−S7 for pulsed laser illumination), shown in Scheme 1a, which was previously used to describe the photophysical processes in various perovskites.[36,37] This allows us to quantitatively extract the carrier mobilities, trap densities, and recombination rates in CsMAFA. The fits are added to Figure 2a with solid lines (see Figure S10a for longer time scales) and match the experimental traces well. In Table 1 the

Table 1. Rate Constants, Trap Densities, and Mobilities Extracted from the Fits to TRMC traces of CsMAFA, C60/CsMAFA, and CsMAFA/C60 Bilayers

	CsMAFA	C60/CsMAFA	CsMAFA/C60
k_2 ($\times 10^{-9}$ cm^3 s^{-1})	3.5	3.5	3.5
k_T ($\times 10^{-9}$ cm^3 s^{-1})	5	5	5
k_D ($\times 10^{-9}$ cm^3 s^{-1})	0.5	0.5	0.5
N_T ($\times 10^{13}$ cm^{-3})	6.5	6.5	6.5
p_0 ($\times 10^{13}$ cm^{-3})	0.8	0.8	0.8
μ_e (cm^2/(Vs))	14	14	14
μ_h (cm^2/(Vs))	14	14	14
k_{ext} ($\times 10^7$ s^{-1})	–	6	6
k_{rec} ($\times 10^7$ s^{-1})	–	0.06	0.6

kinetic parameters are collected. The second-order recombination rate constant (k_2) is around 3.5 × 10^{-9} cm^3 s^{-1}, in line with the reported value for other high-quality perovskite thin films.[38] Furthermore, the trap density (N_T) is 6.5 × 10^{13} cm^{-3}, which is relatively low for polycrystalline perovskite films. Since the effective masses of electrons and holes are very comparable as shown by density functional theory calculations,[39] we kept the mobilities of electrons and holes identical during the fitting procedure to 14 cm^2/(Vs).

Next, to simulate the TRMC traces under BI, we took both the temporal laser pulse and continuous illumination into account (see Note S2 for the used set of differential equations S7−S9 for pulsed laser and bias illumination), using the same kinetic model and the same set of parameters in Table 1, as has been done for $MAPbI_3$.[40] The detailed global, iterative fitting procedure is summarized in Note S2. The fits were added to the TRMC traces in Figures 2**b, c** (see Figures S10b, c for longer time scales) as solid lines, in excellent agreement with the dashed experimental traces. In Figure 3, the modeled concentrations of holes, electrons, and trapped electrons for a pulsed laser excitation of I_0 = 7 × 10^9 photons/cm^2/pulse (1 × 10^{14} excitations/cm^3/pulse) are shown. Figure 3a displays the carrier concentration generated using only the pulsed laser, showing the temporal evolution of the carriers and traps after the pulse. Under a BI of 0.86 mW (Figure 3b), the carrier concentrations created by the BI and pulsed laser are rather comparable, which means that their carrier dynamics are affected by both sources. When the BI increases to 5 mW (Figure 3c), excess carriers generated by the BI become dominant. Therefore, the carrier decay behavior is governed by the BI, leading to a pseudo-first-order recombination process.

To better understand the differences in carrier extraction dynamics between C60/CsMAFA and CsMAFA/C60, we simulated the TRMC traces in these two bilayers using the same kinetic model but extended it by the introduction of an ETL, to account for the additional charge extraction and recombination pathways, as shown in Scheme 1a in red (see Note S2 for the used differential equation S10). The fits are added as solid lines to the dashed experimental data in Figure 1b and Figure 1g, respectively. Note that we used the same set

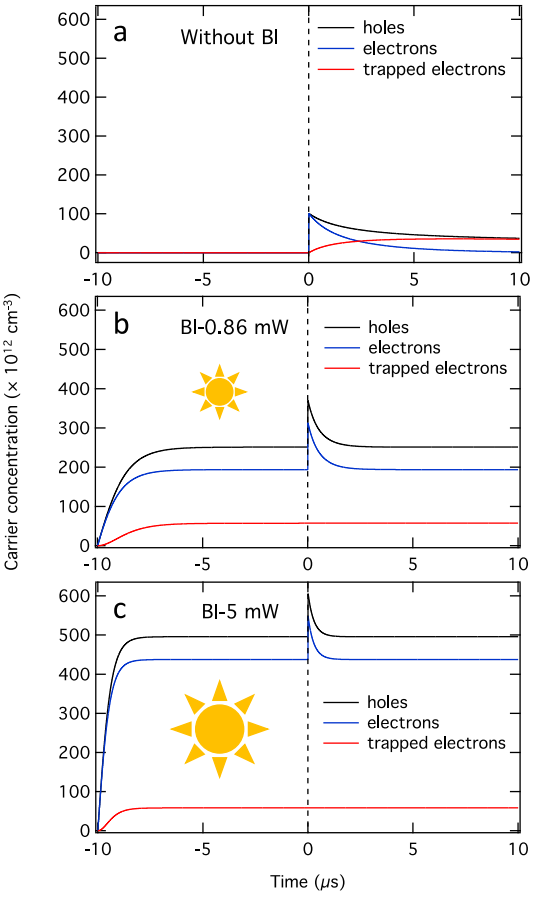

Figure 3. Modeling of the charge carrier concentration using the pulsed laser with an incident fluence of 7 × 10^9 photons/cm^2/pulse (a) or a combination of pulsed and biased illumination sources under different BI intensities (b, c) in the neat CsMAFA layer.

of parameters obtained from the fit of neat CsMAFA, leaving only k_{ext} and k_{rec} to vary. The results are added to Table 1. The carrier extraction rate, k_{ext}, for both bilayers is found to amount to 6 × 10^7 s^{-1}, in agreement with previously reported values.[30,40] Interestingly, the recombination time constant, k_{rec} is 10 times larger in CsMAFA/C60 than that in C60/CsMAFA. This implies that for the former bilayer, carrier recombination is likely to proceed via trap-mediated pathways, as indicated by the dashed arrows in Scheme 1a, when C60 is deposited on top of CsMAFA. Therefore, the sequence of deposition seems to be important for the formation of interfacial states between CsMAFA and C60.

Finally, we want to see how charge collection and recombination at the interface affect the quasi-Fermi level splitting (QFLS), which is a measure of the possible attainable open circuit voltage. We derived the QFLS from steady-state microwave conductivity measurements under simulated sunlight (see the Experimental methods and Note S3 in the Supporting Information for details). Figure 4 shows the measured QFLS for a bare CsMAFA layer and various bi- and triple-layers under AM 1.5 illumination. The QFLS of the neat CsMAFA layer is approximately 1.17 eV, which is close to the previously reported QFLS values derived from the PLQY (~1.2 eV) and the V_{OC} obtained on FA-rich PSCs (1.13−1.18 eV).[15,17,18,41] For the CsMAFA/C60 showing short-lived charge separation, implying electron collection is followed by

https://doi.org/10.1021/acsenergylett.4c00250
ACS Energy Lett. 2024, 9, 2456−2463

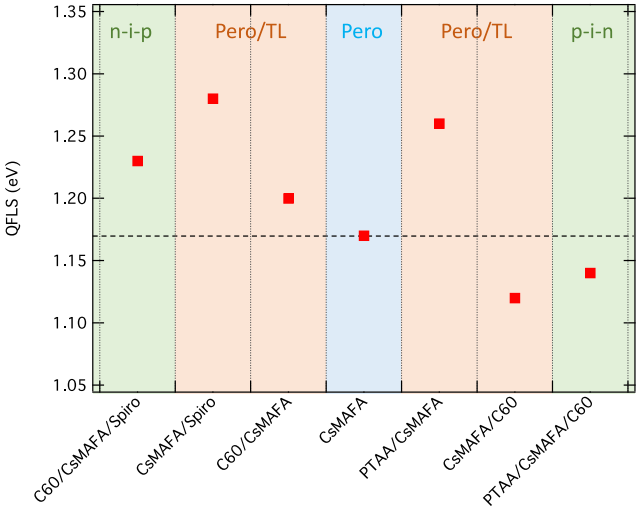

Figure 4. Calculated QFLS of the neat CsMAFA layer (blue shade) and combined with hole or electron transport layers (orange shade) as well as the corresponding n-i-p and p-i-n stacks (green shade) derived from the steady-state microwave conductivity measurement.

rapid interfacial recombination through multiple possible processes as shown by the red arrows in Scheme 1a. Hence the corresponding QFLS is reduced with respect to the pristine CsMAFA layer. Most importantly, for the other bilayer combinations including in C60/CsMAFA long-lived charge separation is observed which translates into an increase of the QFLS with respect to the CsMAFA layer. We attribute this to the passivation effect at the C60/CsMAFA or CsMAFA/Spiro interface. Therefore, the QFLS measurements imply that interfacial recombination by trapping does not play a dominant role in the n/i and i/p interfaces. Furthermore, the n-i-p and p-i-n stacks were evaluated. Compared to the n-i-p configuration, the QFLS of the p-i-n structure is significantly lower, suggesting that again the CsMAFA/C60 interface is likely to be the major issue limiting the final V_{OC} of the device. Therefore, the inclusion of an interfacial layer might indeed be important to obtain long-lived charge separation in CsMAFA/C60 bilayers.[11] The origin of the losses is not well-known and might be due to the deposition conditions used for the C60 layer or the impact of the collision of the C60 molecules with the perovskite surface. A recent study claimed that this interfacial recombination most likely occurs within the first monolayer of C60 at the interface.[20] Future research on fundamental aspects may help to understand more about the origins of these losses.

To summarize, in this Letter, we performed TRMC measurements in single, double, and triple layers comprising a triple-cation lead mixed-halide perovskite absorber layer (CsMAFA), C60 as ETL and Spiro-OMeTAD (n-i-p) or PTAA (p-i-n) as HTL. From the analysis of the bilayers, charge extraction from CsMAFA to Spiro and PTAA is efficient, demonstrating long-lived charge separation. The recombination in CsMAFA/C60 is much faster than in C60/CsMAFA, implying the presence of interfacial trap states when C60 is deposited on top of CsMAFA. The sequence of deposition seems to be important for the formation of these interfacial states which should be reduced to increase the Fermi level splitting and subsequently the V_{OC} of a corresponding solar cell. Furthermore, the similar reduction of the TRMC signal in CsMAFA/ETL and CsMAFA/HTL bilayers compared to neat CsMAFA indicates that the mobilities of electrons and holes are balanced in the perovskite. In trilayer systems, a strongly decreased TRMC signal is observed for both n-i-p and p-i-n stacks indicating efficient charge carrier extraction. At higher incident intensities, the charge asymmetry caused by charge extraction leads to an internal electric field, which is opposite to the direction of the charge extraction, increasing the TRMC signal. Applying BI leads to the formation of an equilibrium of electrons and holes in both TLs. Interestingly, recording a TRMC signal results in a much higher signal in the presence of BI than without BI. In fact, with BI, the triple layer resembles the TRMC signal of a bare CsMAFA under the same BI. This provides valuable insight into how charge collection and recombination at the perovskite/TL interfaces affect the performance of PSCs based on FA-rich perovskites.

■ ASSOCIATED CONTENT

Supporting Information

The Supporting Information is available free of charge at https://pubs.acs.org/doi/10.1021/acsenergylett.4c00250.

Experimental methods; XRD pattern, SEM, absorption, PL spectra, TRMC of CsMAFA thin film; energy band diagrams; TRMC fitting differential equations, detailed TRMC measurements, QFLS determination (PDF)

■ AUTHOR INFORMATION

Corresponding Author

Tom J. Savenije − *Department of Chemical Engineering, Faculty of Applied Sciences, Delft University of Technology, 2629 HZ Delft, The Netherlands;* orcid.org/0000-0003-1435-9885; Email: T.J.Savenije@tudelft.nl

Authors

Jiashang Zhao − *Department of Chemical Engineering, Faculty of Applied Sciences, Delft University of Technology, 2629 HZ Delft, The Netherlands*

Lara M. van der Poll − *Department of Chemical Engineering, Faculty of Applied Sciences, Delft University of Technology, 2629 HZ Delft, The Netherlands*

Sander L. Looman − *Department of Chemical Engineering, Faculty of Applied Sciences, Delft University of Technology, 2629 HZ Delft, The Netherlands*

Jin Yan − *Department of Chemical Engineering, Faculty of Applied Sciences, Delft University of Technology, 2629 HZ Delft, The Netherlands; PVMD group, Delft University of Technology, 2628 CD Delft, The Netherlands*

Jos Thieme − *Department of Chemical Engineering, Faculty of Applied Sciences, Delft University of Technology, 2629 HZ Delft, The Netherlands*

Bahiya Ibrahim − *Department of Chemical Engineering, Faculty of Applied Sciences, Delft University of Technology, 2629 HZ Delft, The Netherlands*

Complete contact information is available at: https://pubs.acs.org/10.1021/acsenergylett.4c00250

Notes

The authors declare no competing financial interest.

https://doi.org/10.1021/acsenergylett.4c00250
ACS Energy Lett. 2024, 9, 2456−2463

■ ACKNOWLEDGMENTS

J.Z. acknowledges the CSC (China Scholarship Council) for funding, File No. 201906360169. L.P. acknowledges HyET Solar for funding.

■ REFERENCES

(1) Stranks, S. D.; Eperon, G. E.; Grancini, G.; Menelaou, C.; Alcocer, M. J. P.; Leijtens, T.; Herz, L. M.; Petrozza, A.; Snaith, H. J. Electron-Hole Diffusion Lengths Exceeding 1 Micrometer in an Organometal Trihalide Perovskite Absorber. *Science* **2013**, *342* (6156), 341−344.

(2) Grätzel, M. The Light and Shade of Perovskite Solar Cells. *Nat. Mater.* **2014**, *13* (9), 838−842.

(3) Li, Z.; Li, B.; Wu, X.; Sheppard, S. A.; Zhang, S.; Gao, D.; Long, N. J.; Zhu, Z. Organometallic-Functionalized Interfaces for Highly Efficient Inverted Perovskite Solar Cells. *Science* **2022**, *376* (6591), 416−420.

(4) Fu, G.; Lee, D.-K.; Ma, C.; Park, N.-G. Disulfidation Interfacial Engineering toward Stable, Lead-Immobilizable Perovskite Solar Cells. *ACS Energy Lett.* **2023**, *8*, 4563−4571.

(5) Li, Y.; Xie, H.; Lim, E. L.; Hagfeldt, A.; Bi, D. Recent Progress of Critical Interface Engineering for Highly Efficient and Stable Perovskite Solar Cells. *Adv. Energy Mater.* **2022**, *12* (5), 1−31.

(6) Tan, H.; Jain, A.; Voznyy, O.; Lan, X.; De Arquer, F. P. G.; Fan, J. Z.; Quintero-Bermudez, R.; Yuan, M.; Zhang, B.; Zhao, Y.; Fan, F.; Li, P.; Quan, L. N.; Zhao, Y.; Lu, Z. H.; Yang, Z.; Hoogland, S.; Sargent, E. H. Efficient and Stable Solution-Processed Planar Perovskite Solar Cells via Contact Passivation. *Science* **2017**, *355* (6326), 722−726.

(7) Tennyson, E. M.; Doherty, T. A. S.; Stranks, S. D. Heterogeneity at Multiple Length Scales in Halide Perovskite Semiconductors. *Nat. Rev. Mater.* **2019**, *4* (9), 573−587.

(8) Park, N. G.; Zhu, K. Scalable Fabrication and Coating Methods for Perovskite Solar Cells and Solar Modules. *Nat. Rev. Mater.* **2020**, *5* (5), 333−350.

(9) Chen, H.; Maxwell, A.; Li, C.; Teale, S.; Chen, B.; Zhu, T.; Ugur, E.; Harrison, G.; Grater, L.; Wang, J.; Wang, Z.; Zeng, L.; Park, S. M.; Chen, L.; Serles, P.; Awni, R. A.; Subedi, B.; Zheng, X.; Xiao, C.; Podraza, N. J.; Filleter, T.; Liu, C.; Yang, Y.; Luther, J. M.; De Wolf, S.; Kanatzidis, M. G.; Yan, Y.; Sargent, E. H. Regulating Surface Potential Maximizes Voltage in All-Perovskite Tandems. *Nature* **2023**, *613* (7945), 676−681.

(10) Gottesman, R.; Lopez-Varo, P.; Gouda, L.; Jimenez-Tejada, J. A.; Hu, J.; Tirosh, S.; Zaban, A.; Bisquert, J. Dynamic Phenomena at Perovskite/Electron-Selective Contact Interface as Interpreted from Photovoltage Decays. *Chem.* **2016**, *1* (5), 776−789.

(11) Mariotti, S.; Köhnen, E.; Scheler, F.; Sveinbjörnsson, K.; Zimmermann, L.; Piot, M.; Yang, F.; Li, B.; Warby, J.; Musiienko, A.; Menzel, D.; Lang, F.; Keßler, S.; Levine, I.; Mantione, D.; Al-Ashouri, A.; Härtel, M. S.; Xu, K.; Cruz, A.; Kurpiers, J.; Wagner, P.; Köbler, H.; Li, J.; Magomedov, A.; Mecerreyes, D.; Unger, E.; Abate, A.; Stolterfoht, M.; Stannowski, B.; Schlatmann, R.; Korte, L.; Albrecht, S. Interface Engineering for High-Performance, Triple-Halide Perovskite-Silicon Tandem Solar Cells. *Science* **2023**, *381* (6653), 63−69.

(12) Zhu, H.; Liu, Y.; Eickemeyer, F. T.; Pan, L.; Ren, D.; Ruiz-Preciado, M. A.; Carlsen, B.; Yang, B.; Dong, X.; Wang, Z.; Liu, H.; Wang, S.; Zakeeruddin, S. M.; Hagfeldt, A.; Dar, M. I.; Li, X.; Grätzel, M. Tailored Amphiphilic Molecular Mitigators for Stable Perovskite Solar Cells with 23.5% Efficiency. *Adv. Mater.* **2020**, *32* (12), 1−8.

(13) Wolff, C. M.; Caprioglio, P.; Stolterfoht, M.; Neher, D. Nonradiative Recombination in Perovskite Solar Cells: The Role of Interfaces. *Adv. Mater.* **2019**, *31* (52), 1902762.

(14) NREL. Best Research-Cell Efficiency Chart. https://www.nrel.gov/pv/cell-efficiency.html (accessed 2024-03-14).

(15) Li, G.; Su, Z.; Canil, L.; Hughes, D.; Aldamasy, M. H.; Dagar, J.; Trofimov, S.; Wang, L.; Zuo, W.; Jerónimo-Rendon, J. J.; Byranvand, M. M.; Wang, C.; Zhu, R.; Zhang, Z.; Yang, F.; Nasti, G.; Naydenov, B.; Tsoi, W. C.; Li, Z.; Gao, X.; Wang, Z.; Jia, Y.; Unger, E.; Saliba, M.; Li, M.; Abate, A. Highly Efficient P-i-n Perovskite Solar Cells That Endure Temperature Variations. *Science* **2023**, *379* (6630), 399−403.

(16) Guo, D.; Caselli, V. M.; Hutter, E. M.; Savenije, T. J. Comparing the Calculated Fermi Level Splitting with the Open-Circuit Voltage in Various Perovskite Cells. *ACS Energy Lett.* **2019**, *4* (4), 855−860.

(17) Stolterfoht, M.; Caprioglio, P.; Wolff, C. M.; Márquez, J. A.; Nordmann, J.; Zhang, S.; Rothhardt, D.; Hörmann, U.; Amir, Y.; Redinger, A.; Kegelmann, L.; Zu, F.; Albrecht, S.; Koch, N.; Kirchartz, T.; Saliba, M.; Unold, T.; Neher, D. The Impact of Energy Alignment and Interfacial Recombination on the Internal and External Open-Circuit Voltage of Perovskite Solar Cells. *Energy Environ. Sci.* **2019**, *12* (9), 2778−2788.

(18) Caprioglio, P.; Stolterfoht, M.; Wolff, C. M.; Unold, T.; Rech, B.; Albrecht, S.; Neher, D. On the Relation between the Open-Circuit Voltage and Quasi-Fermi Level Splitting in Efficient Perovskite Solar Cells. *Adv. Energy Mater.* **2019**, *9* (33), 1901631.

(19) Haddad, J.; Krogmeier, B.; Klingebiel, B.; Krückemeier, L.; Melhem, S.; Liu, Z.; Hüpkes, J.; Mathur, S.; Kirchartz, T. Analyzing Interface Recombination in Lead-Halide Perovskite Solar Cells with Organic and Inorganic Hole-Transport Layers. *Adv. Mater. Interfaces* **2020**, *7* (16), 2000366.

(20) Warby, J.; Zu, F.; Zeiske, S.; Gutierrez-Partida, E.; Frohloff, L.; Kahmann, S.; Frohna, K.; Mosconi, E.; Radicchi, E.; Lang, F.; Shah, S.; Peña-Camargo, F.; Hempel, H.; Unold, T.; Koch, N.; Armin, A.; De Angelis, F.; Stranks, S. D.; Neher, D.; Stolterfoht, M. Understanding Performance Limiting Interfacial Recombination in Pin Perovskite Solar Cells. *Adv. Energy Mater.* **2022**, *12* (12), 1−10.

(21) Serpetzoglou, E.; Konidakis, I.; Kakavelakis, G.; Maksudov, T.; Kymakis, E.; Stratakis, E. Improved Carrier Transport in Perovskite Solar Cells Probed by Femtosecond Transient Absorption Spectroscopy. *ACS Appl. Mater. Interfaces* **2017**, *9* (50), 43910−43919.

(22) Khan, J. I.; Isikgor, F. H.; Ugur, E.; Raja, W.; Harrison, G. T.; Yengel, E.; Anthopoulos, T. D.; De Wolf, S.; Laquai, F. Charge Carrier Recombination at Perovskite/Hole Transport Layer Interfaces Monitored by Time-Resolved Spectroscopy. *ACS Energy Lett.* **2021**, *6* (12), 4155−4164.

(23) Ugur, E.; Khan, J. I.; Aydin, E.; Wang, M.; Kirkus, M.; Neophytou, M.; McCulloch, I.; De Wolf, S.; Laquai, F. Carrier Extraction from Perovskite to Polymeric Charge Transport Layers Probed by Ultrafast Transient Absorption Spectroscopy. *J. Phys. Chem. Lett.* **2019**, *10* (21), 6921−6928.

(24) Le Corre, V. M.; Stolterfoht, M.; Perdigón Toro, L.; Feuerstein, M.; Wolff, C.; Gil-Escrig, L.; Bolink, H. J.; Neher, D.; Koster, L. J. A. Charge Transport Layers Limiting the Efficiency of Perovskite Solar Cells: How to Optimize Conductivity, Doping, and Thickness. *ACS Appl. Energy Mater.* **2019**, *2* (9), 6280−6287.

(25) Ravishankar, S.; Gharibzadeh, S.; Roldán-Carmona, C.; Grancini, G.; Lee, Y.; Ralaiarisoa, M.; Asiri, A. M.; Koch, N.; Bisquert, J.; Nazeeruddin, M. K. Influence of Charge Transport Layers on Open-Circuit Voltage and Hysteresis in Perovskite Solar Cells. *Joule* **2018**, *2* (4), 788−798.

(26) Hutter, E. M.; Kirchartz, T.; Ehrler, B.; Cahen, D.; Von Hauff, E. Pitfalls and Prospects of Optical Spectroscopy to Characterize Perovskite-Transport Layer Interfaces. *Appl. Phys. Lett.* **2020**, *116* (10), 100501.

(27) Bisquert, J.; Janssen, M. From Frequency Domain to Time Transient Methods for Halide Perovskite Solar Cells: The Connections of IMPS, IMVS, TPC, and TPV. *J. Phys. Chem. Lett.* **2021**, *12* (33), 7964−7971.

(28) Bisquert, J. Interpretation of the Recombination Lifetime in Halide Perovskite Devices by Correlated Techniques. *J. Phys. Chem. Lett.* **2022**, *13* (31), 7320−7335.

(29) Lopez-Varo, P.; Jiménez-Tejada, J. A.; García-Rosell, M.; Anta, J. A.; Ravishankar, S.; Bou, A.; Bisquert, J. Effects of Ion Distributions on Charge Collection in Perovskite Solar Cells. *ACS Energy Lett.* **2017**, *2* (6), 1450−1453.

https://doi.org/10.1021/acsenergylett.4c00250
ACS Energy Lett. 2024, 9, 2456−2463

(30) Hutter, E. M.; Hofman, J. J.; Petrus, M. L.; Moes, M.; Abellón, R. D.; Docampo, P.; Savenije, T. J. Charge Transfer from Methylammonium Lead Iodide Perovskite to Organic Transport Materials: Efficiencies, Transfer Rates, and Interfacial Recombination. *Adv. Energy Mater.* **2017**, *7* (13), 1−8.
(31) Caselli, V. M.; Wei, Z.; Ackermans, M. M.; Hutter, E. M.; Ehrler, B.; Savenije, T. J. Charge Carrier Dynamics upon Sub-Bandgap Excitation in Methylammonium Lead Iodide Thin Films: Effects of Urbach Tail, Deep Defects, and Two-Photon Absorption. *ACS Energy Lett.* **2020**, *5* (12), 3821−3827.
(32) Zhao, J.; Liu, X.; Wu, Z.; Ibrahim, B.; Thieme, J.; Brocks, G.; Tao, S.; Bannenberg, L. J.; Savenije, T. J. Temperature-Dependent Interplay between Structural and Charge Carrier Dynamics in CsMAFA-Based Perovskites. *Adv. Funct. Mater.* **2024**, *34*, 2311727.
(33) Hutter, E. M.; Eperon, G. E.; Stranks, S. D.; Savenije, T. J. Charge Carriers in Planar and Meso-Structured Organic-Inorganic Perovskites: Mobilities, Lifetimes, and Concentrations of Trap States. *J. Phys. Chem. Lett.* **2015**, *6* (15), 3082−3090.
(34) Savenije, T. J.; Guo, D.; Caselli, V. M.; Hutter, E. M. Quantifying Charge-Carrier Mobilities and Recombination Rates in Metal Halide Perovskites from Time-Resolved Microwave Photoconductivity Measurements. *Adv. Energy Mater.* **2020**, *10* (26), 1903788.
(35) Al-Ashouri, A.; Köhnen, E.; Li, B.; Magomedov, A.; Hempel, H.; Caprioglio, P.; Márquez, J. A.; Vilches, A. B. M.; Kasparavicius, E.; Smith, J. A.; Phung, N.; Menzel, D.; Grischek, M.; Kegelmann, L.; Skroblin, D.; Gollwitzer, C.; Malinauskas, T.; Jošt, M.; Matič, G.; Rech, B.; Schlatmann, R.; Topič, M.; Korte, L.; Abate, A.; Stannowski, B.; Neher, D.; Stolterfoht, M.; Unold, T.; Getautis, V.; Albrecht, S. Monolithic Perovskite/Silicon Tandem Solar Cell with > 29% Efficiency by Enhanced Hole Extraction. *Science* **2020**, *370* (6522), 1300−1309.
(36) Hutter, E. M.; Eperon, G. E.; Stranks, S. D.; Savenije, T. J. Charge Carriers in Planar and Meso-Structured Organic-Inorganic Perovskites: Mobilities, Lifetimes, and Concentrations of Trap States. *J. Phys. Chem. Lett.* **2015**, *6* (15), 3082−3090.
(37) Guo, D.; Andaji Garmaroudi, Z.; Abdi-Jalebi, M.; Stranks, S. D.; Savenije, T. J. Reversible Removal of Intermixed Shallow States by Light Soaking in Multication Mixed Halide Perovskite Films. *ACS Energy Lett.* **2019**, *4* (10), 2360−2367.
(38) Davies, C. L.; Filip, M. R.; Patel, J. B.; Crothers, T. W.; Verdi, C.; Wright, A. D.; Milot, R. L.; Giustino, F.; Johnston, M. B.; Herz, L. M. Bimolecular Recombination in Methylammonium Lead Triiodide Perovskite Is an Inverse Absorption Process. *Nat. Commun.* **2018**, *9* (1), 1−9.
(39) Galkowski, K.; Mitioglu, A.; Miyata, A.; Plochocka, P.; Portugall, O.; Eperon, G. E.; Wang, J. T. W.; Stergiopoulos, T.; Stranks, S. D.; Snaith, H. J.; Nicholas, R. J. Determination of the Exciton Binding Energy and Effective Masses for Methylammonium and Formamidinium Lead Tri-Halide Perovskite Semiconductors. *Energy Environ. Sci.* **2016**, *9* (3), 962−970.
(40) Caselli, V. M.; Savenije, T. J. Quantifying Charge Carrier Recombination Losses in MAPbI3/C60 and MAPbI3/Spiro-OMeTAD with and without Bias Illumination. *J. Phys. Chem. Lett.* **2022**, *13* (32), 7523−7531.
(41) You, S.; Zeng, H.; Liu, Y.; Han, B.; Li, M.; Li, L.; Zheng, X.; Guo, R.; Luo, L.; Li, Z.; Zhang, C.; Liu, R.; Zhao, Y.; Zhang, S.; Peng, Q.; Wang, T.; Chen, Q.; Eickemeyer, F. T.; Carlsen, B.; Zakeeruddin, S. M.; Mai, L.; Rong, Y.; Grätzel, M.; Li, X. Radical Polymeric P-Doping and Grain Modulation for Stable, Efficient Perovskite Solar Modules. *Science* **2023**, *379* (6629), 288−294.

https://doi.org/10.1021/acsenergylett.4c00250
ACS Energy Lett. 2024, 9, 2456−2463